Clinical Neurophysiology 122 (2011) 134–147

Contents lists available at ScienceDirect

Clinical Neurophysiology

journal homepage: www.elsevier.com/locate/clinph

Model-based analysis and quantification of age trends in auditory evoked potentials

C.C. Kerr [a,b,*], C.J. Rennie [a,b,c], P.A. Robinson [a,b,d]

[a] School of Physics, University of Sydney, New South Wales 2006, Australia
[b] Brain Dynamics Centre, Westmead Millennium Institute, Sydney Medical School – Western, University of Sydney, Westmead Hospital, New South Wales 2145, Australia
[c] Department of Medical Physics, Westmead Hospital, Westmead, New South Wales 2145, Australia
[d] Sydney Medical School, University of Sydney, New South Wales 2006, Australia

ARTICLE INFO

Article history:
Accepted 15 May 2010
Available online 1 July 2010

Keywords:
Auditory oddball
Evoked potentials
Continuum modeling
Thalamocortical interactions
Development and aging
N1
N2
P2
P3

ABSTRACT

Objective: The physiological basis for the changes in auditory evoked potentials (AEPs) during development and aging is currently unknown. This study investigates age- and task-related changes via a mathematical model of neuronal activity, which allows a number of physiological changes to be inferred.
Methods: A quantitative, physiology-based model of activity in cortical and thalamic neurons was used to analyze oddball AEPs recorded from 1498 healthy subjects aged 6–86 years.
Results: Differences between standard and target responses can be largely explained by differences in connection strengths between thalamic and cortical neurons. The time it takes signals to travel between the thalamus and cortex decreases during development and increases during aging. Strong age trends are also seen in intracortical and thalamocortical neuronal connection strengths.
Conclusions: Changes in AEP latency can be attributed to changes in the thalamocortical signal propagation time. Large changes in the connection strengths between neuronal populations occur during development, resulting in increased thalamocortical inhibition and decreased thalamocortical excitation. Standard and target parameters are similar in children but diverge during adolescence, due to changes in thalamocortical loop activity.
Significance: Model-based AEP analysis links age-related changes in brain electrophysiology to underlying changes in brain anatomy and physiology, and yields quantitative predictions of several currently unknown physiological and anatomical properties of the brain.

1. Introduction

Studies of age trends in auditory evoked potentials (AEPs) have relied almost exclusively on phenomenological methods of analysis, such as component scoring. Although these studies provide tantalizing clues to developmental and aging trends, they have provided little information on the actual physiology underlying these changes. Our aim is to gain insight into the changes in the brain during development and aging by applying a physiology-based model of neuronal activity to oddball AEP waveforms, obtained from a very large sample of healthy subjects across a wide age range.

Component scoring of AEPs has yielded conflicting results for both developing and aging trends; these trends were investigated in Kerr et al. (2010) for the same 1498 subjects as used in this study. Only two component scores, target N2 and P3 latencies, show age trends that have been both consistently and widely reported. Target P3 latency decreases by 5–19 ms/year during development (Oades et al., 1997; Barajas, 1990), and increases by 0.6–3 ms/year during aging (Brown et al., 1983; Kerr et al., 2010). Target N2 latency decreases by 2–12 ms/year during development (Johnstone et al., 1996; Goodin et al., 1978) and increases by 0.5–1.4 ms/year during aging (Bahramali et al., 1999; Brown et al., 1983). One significant limitation of component scoring is that changes in amplitude can produce changes in latency, and vice versa, due to the superposition of adjacent components (Kerr et al., 2009).

Component scoring has been augmented by dipole modeling, which in principle allows additional spatiotemporal information to be obtained about the intracortical sources of the AEP. While the inverse problem of EEG source localization has no unique solution (Nunez, 1995), additional assumptions such as parsimony of sources and smooth changes in activity allow source location estimates to be made (Scherg and Von Cramon, 1986). Dipole studies are limited in that they require restrictive assumptions about the number, location, and nature of the sources – assumptions that are largely unconfirmed experimentally (for example, combined fMRI and dipole studies often find somewhat different source localizations; see (Scarff et al., 2004)). Although dipole modeling

* Corresponding author at: School of Physics, University of Sydney, New South Wales 2006, Australia. Tel.: +61 412 038 402; fax: +61 2 9351 7726.
E-mail address: ckerr@physics.usyd.edu.au (C.C. Kerr).

1388-2457/$36.00
doi:10.1016/j.clinph.2010.05.030

provides more detailed information on anatomy than other methods, it is limited in the additional information about physiology it can provide, except in terms of temporal source separation, for which more specific methods exist, such as independent component analysis (Makeig et al., 2002). Nonetheless, several interesting findings have been obtained using dipole modeling. Albrecht et al. (2000) found similar source localizations in both children and adults; the main age differences were the absence of the N1/P2 complex and longer component latencies in children. Ponton et al. (2002) also found no changes in source location, but unlike Albrecht et al. (2000), they found stronger developmental effects on amplitude than latency. In contrast, Čeponienė et al. (2002) found evidence that dipole sources do change location between children and adults, at least for N1.

At least four important changes occur in brain anatomy and physiology during the developmental period investigated in this study (ages 6–20), even though the brain has already reached nearly adult size by age 6 (Lenroot and Giedd, 2006). First, myelination increases rapidly during childhood, and then more slowly through adolescence and early adulthood, such that the total amount of myelin nearly doubles between birth and age 20, at least in some regions of the brain (Benes et al., 1994). Second, gray matter density first increases and then decreases during childhood and adolescence, due to changes in synapse number and/or cell size (Giedd et al., 1999). There is a strong correlation between increasing white matter volume and decreasing gray matter density (Sowell et al., 2004), and different cortical areas mature at different rates: primary sensorimotor areas mature earlier than association areas (Giedd, 2008), with the dorsolateral prefrontal cortex among the last to mature (Lenroot and Giedd, 2006). Additional developmental changes include maturation of the neurofilaments of the axons in the superficial cortical layers (I–III) between the ages 5 and 12 (Moore and Guan, 2001), and possible increases in the activity of the dopaminergic neuromodulatory system through to adolescence (de Graaf-Peters and Hadders-Algra, 2006).

The anatomical and physiological changes in the brain during aging are more straightforward. There is substantial evidence that loss of and/or damage to the myelin sheaths occurs (Peters, 2002; Piguet et al., 2009), especially for small-diameter fibers (Marner et al., 2003), and especially in the frontal cortex (Sowell et al., 2004). This process begins at age 40–50 and accelerates with increasing age (Sowell et al., 2004). Gray matter loss during aging is also most pronounced in the frontal cortex (Bartzokis et al., 2001), and is thought to result primarily from cell shrinkage and synaptic pruning, rather than actual cell loss (Sowell et al., 2004). Changes in chemical signaling systems also occur during aging, including decreased activity in both dopaminergic (Volkow et al., 2000) and cholinergic systems (Gallagher and Colombo, 1995).

Links between age-related changes in AEPs and age-related changes in anatomy or physiology have tended to be highly speculative, since the correspondence between scalp potentials and the neural mechanisms underlying them is indirect and incompletely understood. To help bridge this gap, we apply the Robinson et al. (1997, 2001) model to auditory oddball EP time series, thereby allowing estimates to be made of difficult-to-measure physiological quantities. This mathematical model, based on experimentally measured anatomical and physiological properties of the brain, describes the dynamics of, and interactions between, populations of neurons in the cortex and thalamus (Rennie et al., 2002; Robinson et al., 2002). This model builds in part on earlier models, such as those of Wilson and Cowan (1973), Nunez (1974), Freeman (1975), Steriade et al. (1990) and Wright and Liley (1996); however, in contrast to these related models, the Robinson et al. model has no unconstrained parameters, and each parameter corresponds to a particular physiological quantity. This model has previously yielded successes in explaining EEG spectra (Rowe et al., 2004) and their age trends (van Albada et al., 2010), sleep dynamics (Phillips and Robinson, 2007), seizures (Roberts and Robinson, 2008), and Parkinson's disease (van Albada and Robinson, 2009; van Albada et al., 2009), as well as AEPs (Rennie et al., 2002; Kerr et al., 2008) and a range of other phenomena.

The current model is capable of accounting for all major AEP features across the entire age range, with the exception of target P3b. Reproducing this component would require a substantial increase in the physiological and/or anatomical complexity of the model, and at present there is not compelling evidence that the resultant increase in the model's explanatory power would justify the increase in its complexity. The standard approach in modeling is to investigate comparatively simple models before additional details are introduced; this is the approach we take here, since alternative models of greater complexity would be less parsimonious than the current model. It should also be noted that the purpose of the model is to provide information on the physiological correlates of particular states (e.g., standard versus target responses), not to provide a detailed account of how the transitions between these states occur.

This paper is organized as follows. Section 2 describes the Robinson et al. model and the experimental data used in the study. Section 3 presents the results of fitting the model to the data, and describes the changes in parameter values due to task and age. Section 4 discusses possible physiological interpretations of these results, and compares them to existing literature.

2. Methods

2.1. Experimental data

Auditory oddball EPs were recorded from 1498 subjects (763 males, 735 females) with an age range of 6.1–86.6 years, shown in Fig. 1; the same subjects were recently used in studies of age trends in EEG spectra (van Albada et al., 2010) and AEP component

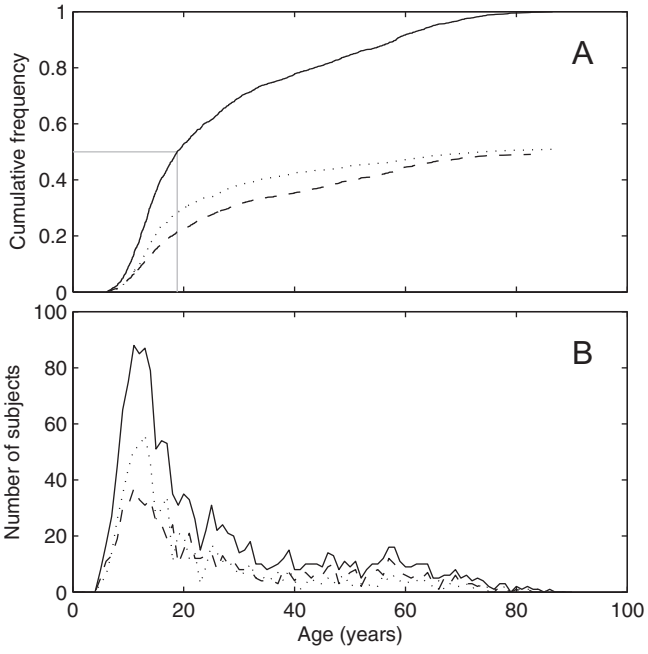

Fig. 1. Cumulative distribution function (A) and density distribution function with one-year age bins (B) of all subjects across age (solid lines). Separate distribution functions for females (dashed lines) and males (dotted lines) are also shown. Approximately half the subjects were under age 19 (A, gray line).

scores and deconvolution quantifications (Kerr et al., 2010). All subjects were healthy, and reported no history of brain injury, disease, or other medical conditions that could influence the normality of the EEG (van Albada et al., 2007). Data collection was done by Brain Resource Ltd. (Ultimo, NSW, Australia; www.brainresource.com) and results made available through the Brain Resource International Database (BRID) (Gordon et al., 2005).

Recordings were made at 26 electrode sites from an extension to the International 10–20 system, following previously published methods for acquisition and artifact removal (Rowe et al., 2004; Gordon et al., 2005). EEG data were recorded at a 500 Hz sampling rate and an A/D precision of 0.06 μV through a NuAmps (Neuroscan) amplifier using an averaged mastoid reference.

Subjects were presented binaurally, via headphones, with a series of standard and target tones (500 and 1000 Hz, respectively), at 75 dB SPL and lasting for 50 ms, with a constant ISI of 1 s, according to a standardized method (Gordon et al., 2005). Subjects were instructed to ignore standard tones, but to respond to target tones with a button press. There were 280 standard (82%) and 60 target (18%) tones presented in pseudorandom order, with the only constraint being that two targets could not appear consecutively. Total task duration was 6 min.

EEG data were corrected offline for eye movements according to a method based on that of Gratton et al. (1983). Only data from the Cz electrode were used for further analysis, as this electrode is relatively unaffected by muscle artifact (Saunders, 1984; Key et al., 2005); a full analysis of the spatial variation in age trends is beyond the scope of this study, and will be the subject of a forthcoming paper. AEP data were extracted from EEG recordings by averaging over a window from 0 to 0.6 s relative to stimulus onset; target and standard responses were averaged separately.

Since single-subject AEP waveforms do not have high enough signal-to-noise ratios for robust model fits, average AEPs were calculated. For investigation of the effects of task condition and for comparison to previous work, adult group average waveforms were computed by averaging over 212 subjects uniformly distributed in age from 20 to 40 years, since age trends are comparatively weak over this range. For investigation of age effects, we used data from all available subjects to estimate smooth life-span trends for each parameter. The 1498 subjects were ranked in order of increasing age, and partitioned into bins of 50 subjects each, with each bin except the first containing 45 subjects from the previous bin and five new subjects. Hence, the full age range was spanned with 290 bins ($50 + 289 \times 5 = 1495$; the remaining three subjects were added to the final bin). The mean age for subjects in the youngest bin was 6.9 years, while it was 78 years for the oldest bin. Average standard and target waveforms for each of the 290 bins were computed by averaging over the 50 subjects in each bin. For investigation of sex differences in age trends, this procedure was also performed on males and females separately.

2.2. Model

The purpose of modeling is to allow estimates to be made of physiological and anatomical properties that are otherwise difficult or impossible to measure noninvasively. Electrical activity measured by a scalp electrode is the result of the activity of tens of millions of neurons; using a suitable model, this scalp activity can be used to provide information on various properties of brain, including the strength of connections between populations of neurons, how long it takes signals to travel between different parts of the brain (e.g., between the cortex and thalamus), and how much of cortex receives direct thalamic input as the result of an auditory stimulus.

The model used here describes how the average neuronal firing rate changes over time in five crucial populations of neurons. As shown in Fig. 2, these populations are: excitatory cortical pyramidal cells (denoted with the subscript e), inhibitory cortical interneurons (i), excitatory thalamic relay nuclei neurons (s), inhibitory thalamic reticular nucleus neurons (r), and excitatory sensory afferents (n). These populations are linked by well-known anatomical connections, also shown in Fig. 2; these include intracortical, intrathalamic, thalamocortical, and corticothalamic projections. Several important spatial aspects of both the cortex and thalamus are incorporated in the model, such as (i) each location in the thalamus projects to a particular location in the cortex, (ii) focal activity in the cortex propagates outwards and decreases in amplitude with distance, and (iii) the time it takes a signal to travel between two regions of cortex is proportional to the distance separating them.

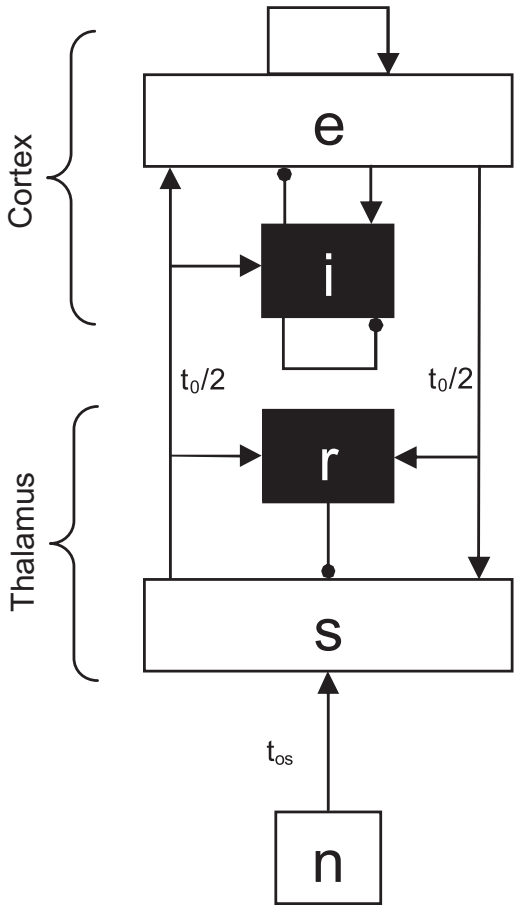

Fig. 2. The Robinson et al. thalamocortical model, consisting of five neuronal populations: cortical excitatory and inhibitory (e and i, respectively), thalamic reticular (r), thalamic sensory (s), and sensory afferents (n). The excitatory and inhibitory populations (white and black boxes, respectively) are linked by known anatomical connections (arrowheads for excitatory connections; circles for inhibitory). Time delays ($t_0/2, t_{os}$) are also shown.

To model evoked potentials, a brief subthalamic impulse is applied to the model, and the model's output (a prediction of the activity in cortical pyramidal cells) is compared to the experimental AEP time series. The model's parameters are then adjusted, and this process is repeated until the output of the model closely matches the experimental data. Since full mathematical detail of the model has been presented elsewhere (Rowe et al., 2004; Kerr et al., 2008), the remainder of this section qualitatively describes the model parameters. These can be divided into network parameters, stimulus parameters, connection strengths, and feedback parameters.

Network parameters describe the properties of individual neurons that are relevant to large neuronal populations (since only large neuronal populations contribute significantly to the EEG signal). The thalamocortical signal propagation time, t_0, is the average

time it takes an impulse to travel from the thalamus to cortex and back. The cortical damping rate, γ, is defined as the axonal propagation velocity v_e divided by the characteristic axonal range r_e, and its reciprocal characterizes the length of time waves of depolarization travel through the cortex before being damped. The parameters β and α are the reciprocals of the rise and decay time constants of the dendritic membrane potential, respectively.

The stimulus reaching the cortex is considered to have a Gaussian profile in both space and time, and is described by five parameters. Its spatial and temporal locations are given by r_{os} and t_{os}, respectively, while its spatial and temporal widths are given by r_s and t_s, respectively. Its amplitude is determined by N; however, this parameter also incorporates the conversion factor between changes in neuronal firing rate and scalp potential, and the strength of the connection from the brainstem to the cortex via the thalamus, since all three of these quantities have no effect other than to scale the waveform.

The strengths of the connections shown in Fig. 2 depend on one anatomical quantity (synapse number) and two physiological ones (neuronal excitability and postsynaptic potential strength). The strength of a connection between two populations of neurons is technically described as a *gain*, called G_{ab}, which is defined as the change in firing rate in neurons of one population (a) divided by the change in firing rate in neurons of other population (b). For example, if a 30% increase in the firing rate of cortical neurons (e) is caused by a 10% increase in the firing rate of thalamic neurons (s), then $G_{es} = 3$. Hence, a gain of one implies equal changes in the firing rates of the two populations, while a negative gain implies inhibition. For example, $G_{ei} = -1$ means that a 10% increase in firing rate of inhibitory cortical neurons i will produce a 10% *decrease* in firing rate of excitatory cortical neurons e. (Note: the physiological foundations of these quantities are described in detail in Robinson et al. (2004).) Gains between more than two populations of neurons are simply the product of the individual gains, written as $G_{ab} \times G_{bc} \equiv G_{abc}$. Hence, although there are 11 connections shown in Fig. 2, these can be combined into five compound gains: excitatory cortical G_{ee}, inhibitory cortical G_{ei}, excitatory thalamocortical G_{ese}, inhibitory thalamocortical G_{esre}, and inhibitory intrathalamic G_{srs}.

By combining these gains, it is possible to define three parameters which characterize the net feedback within different brain regions: X describes corticocortical feedback; Y describes thalamocortical feedback, and Z describes intrathalamic feedback. Additionally, X and Y can be combined into a fourth parameter, S, which contains all five gains, and which describes global feedback. Each of these parameters is associated with an instability of a different frequency in EEG spectra (Robinson et al., 2002). These feedback parameters are listed in Table 1.

2.3. Fitting procedure

As outlined above, the model's response to a brief subthalamic input is fitted to experimental AEP waveforms by varying the model's parameter values. Initial parameter values for fits were obtained by performing preliminary fits to the adult group average target waveform, starting from the parameter values given in Kerr et al. (2008). Initial values and limits were chosen to maximize the following criteria: low χ^2 (weighted sum of squares of residuals) for standard and target fits across all ages, physiological plausibility, and few free parameters. Low χ^2 was used as the primary criterion, up to the point where model fits matched data to within uncertainty in the latter (i.e., ± 2 standard errors). Fits were initially performed with random initializations (as described below), and all parameters were allowed to vary within the constraints provided by physiology (Rowe et al., 2004). A parameter was subsequently fixed if low χ^2 solutions at all ages could be obtained with that parameter set to a constant value.

Table 1
Derived feedback parameters of the model, showing their symbols (first column), the feedback networks that gives rise to them (second column), their definitions (third column), and the most common types of instability they produce when their values are too large (for X, Y, or Z) or small (S).

Parameter	Location	Definition	Instability
X	Cortical	$\frac{G_{ee}}{1-G_{ei}}$	α or θ (4–13 Hz)
Y	Thalamocortical	$\frac{G_{ese}+G_{esre}}{(1-G_{ei})(1-G_{srs})}$	α or θ (4–13 Hz)
Z	Intrathalamic	$-G_{srs}\frac{\alpha\beta}{(\alpha+\beta)^2}$	Spindle (10–15 Hz)
S	Thalamocortical	$1-X-Y$	Baseline (0 Hz)

This procedure determined that the three criteria listed above were best satisfied using five fixed and eight free parameters, with the initial values and limits listed in Table 2. Due to the use of Monte Carlo methods, the choice of initial parameter values had negligible effect on the final fitted values, and hence the initial values of the fitted parameters do not reflect "ideal" or maximum-likelihood values, but instead were chosen to reduce computation time by maximizing the fraction of fits that satisfied the above three criteria.

Prior to fitting, a Monte Carlo method was used to vary the initialization of each parameter, using a uniform distribution of parameter values with a mean equal to the values listed in Table 2 and a range of 40% of the mean. Fitting was performed by adjusting the parameters using the Levenberg–Marquardt method of χ^2 minimization (Press et al., 1992), with χ^2 defined by

$$\chi^2 = \sum_{j=1}^{n} \left(\frac{E(j) - R(j)}{W(j)} \right)^2,$$

where E is the experimental AEP time series, R is the theoretical time series, W is a weight function, j labels data points in the time series, and the sum is over all n data points. The weight function is such that data points are weighted by a factor of 1/4 from 0 to 100 ms, 1 from 100 to 250 ms, 1/2 from 250 to 350 ms, 1/32 from 350 to 500 ms, and 1/512 from 500 to 600 ms. The precise form of the weight function has little effect on the final fits, and its function is primarily to ensure the gradient descent algorithm does not reach a local minimum before fitting the comparatively small number of data points that constitute the target P2–N2 complex. Additionally, the late (350–600 ms) part of the waveform is weighted less heavily during fitting, since ability of the model to fit all features in this range is limited by (i) the approximation that parameter values do not change over the duration of the epoch, and (ii) the restriction in this version of model to the pathways shown in Fig. 2 (Kerr et al., 2008).

The task of finding the optimal set of parameter values is complicated by several factors, including the high dimensionality of parameter space and the fact that it is possible to reproduce certain time series using more than one set of parameters. To obtain a representative sampling of parameter space, the Monte Carlo randomization of the initial parameters and the fitting procedure are repeated several thousand times. Once these fits have been calculated, a subset is selected based on three criteria. First, fits are excluded if their χ^2 value is above a certain threshold, as this indicates that the fit did not find the global minimum. Second, fits are excluded if their parameters produce instability in the model (i.e., activity that grows exponentially with time), since the linear model used here is only valid for stable steady states. Third, fits are rejected if any of their parameters are unphysical or have values outside physiologically accepted limits.

The result of applying these selection criteria is that the parameter distributions are unimodal and approximately Gaussian,

Table 2
Initial values and limits of model parameters used for fitting both standard and targets AEPs. Parameters whose limits are not given are fixed at the initial value. Parameter definitions are provided in Section 2.2.

Parameter	Description	Initial	Minimum	Maximum	Unit
γ	Cortical damping rate	400	–	–	s^{-1}
α	Dendritic rate constant	12	–	–	s^{-1}
N	Amplitude normalization	10	1	10	μV
t_0	Thalamocortical signal propagation time	75	40	100	ms
t_{os}	Temporal stimulus offset	15	–	–	ms
t_s	Temporal stimulus width	10	–	–	ms
r_{os}	Spatial stimulus offset	150	–	–	mm
r_s	Spatial stimulus width	40	1	200	mm
G_{ee}	Cortical excitatory gain	1.0	0.0	15	–
G_{ei}	Cortical inhibitory gain	−9.0	−15	0.0	–
G_{ese}	Thalamocortical excitatory gain	9.0	0.0	15	–
G_{esre}	Thalamocortical inhibitory gain	−1.0	−15	0.0	–
G_{srs}	Intrathalamic inhibitory gain	−3.5	−15	0.0	–

which allows each distribution to be characterized by its mean value and standard deviation (SD). The parameters of these remaining trials are averaged to obtain an estimated value and uncertainty for each parameter. Uncertainties in parameters are largely determined by the size of the region of parameter space capable of producing acceptable fits, and it has been found empirically that one SD can be used as an estimate of this size (Kerr et al., 2008). Hence, while not statistically exact, parameter uncertainty can be estimated as ±1 SD for fits to single waveforms (as in Table 3).

2.4. Age regression analysis

Previous studies of age trends have either used linear or exponential forms, in which case separate lines of best fit are used for development and aging, or a single quadratic form over the full age range. However, none of these appears to match the form of the actual age trends, which instead: (i) appear to be linear at very young and old ages, (ii) change smoothly between development and aging trends, and (iii) have at most one change in slope. One of the simplest functions that meets all three requirements is given by (van Albada et al., 2010; Kerr et al., 2010):

$$y = Cx + \tau(C-A)\ln\left(1+\exp\left[\frac{I-x}{\tau}\right]\right) + D,$$

$$I = \frac{B-D}{C-A},$$

where x represents the age, τ is the width of the transition region between young and old ages, and A, B, C, and D are fitted variables. Although seemingly complicated, this formula merely describes a smooth interpolation between two straight lines which intersect at age I. Goodness-of-fit is relatively insensitive to the parameter τ, so it was set to equal three years in all fits. In Fig. 3, the fitting function used here is compared with the three alternative functions described above, showing that this function most closely matches experimentally observed age trends.

Since the variables A and C describe the slope of the function at the "ages" $-\infty$ and ∞, respectively, we instead report a "development" slope, S_6, which is the slope of the line of best fit at age 6, and an "aging" slope, S_{86}, which is the slope of the line of best fit at age 86. Note that in most cases A and C are very similar to S_6 and S_{86}, respectively, so this correction is usually negligible. In addition to these development and aging slopes, we report M, the median value obtained from fits to waveforms in the age range 20–40, when age-related changes are minimal. Finally, we report I, since it corresponds to the age at which the age trend changes most rapidly. In cases where there is no clear change between development and aging trends, I cannot be calculated.

In order to track the median rather than the mean, fits were performed by minimizing the mean absolute difference, rather than squared deviations, between the line of best fit and the data. Optimization was achieved using a downhill simplex method (Nelder and Mead, 1965). Confidence intervals and standard errors for the variables and fits were obtained by bootstrapping with 1000 resamplings.

Table 3
Group average values and standard deviations (SD) for standard and target parameters (columns 2 and 3). Previously reported parameters for eyes-closed EEG fits (column 4) and standard fits (column 5) are provided for comparison (Kerr et al., 2008).

Parameter	Group average fits		Kerr et al. (2008)	
	Standard (±SD)	Target (±SD)	EEG (±SD)	Standard (±SD)
N (μV)	5.0 ± 2.4	9.0 ± 1.5	–	–
t_0 (ms)	71 ± 15	67 ± 5	84 ± 14	64 ± 4
r_s (mm)	47 ± 19	40 ± 7	–	90 ± 90
G_{ee}	3.1 ± 2.1	1.1 ± 1.5	5.6 ± 3.8	3.1 ± 1.6
G_{ei}	−10.7 ± 3.0	−8.5 ± 2.6	−6.9 ± 3.9	−10.8 ± 1.7
G_{ese}	0.3 ± 0.7	8.6 ± 2.8	7.7 ± 5.0	0.8 ± 0.7
G_{esre}	−5.5 ± 2.3	−13.3 ± 2.2	−5.3 ± 4.2	−7.8 ± 2.1
G_{srs}	−4.2 ± 0.6	−3.0 ± 1.0	−0.8 ± 0.5	−0.8 ± 0.1
X	0.3 ± 0.2	0.1 ± 0.1	0.7 ± 0.2	0.3 ± 0.1
Y	−0.08 ± 0.04	−0.2 ± 0.1	0.2 ± 0.2	−0.3 ± 0.1
Z	0.35 ± 0.05	0.24 ± 0.08	0.1 ± 0.1	0.1 ± 0.1
S	0.8 ± 0.2	1.1 ± 0.2	0.1 ± 0.1	1.1 ± 0.2

3. Results

3.1. Group average adult fits

This section describes fits to the group average standard and target waveforms of the 212 adults aged 20–40 years; parameters of these fits are listed in Table 3. Goodness-of-fit of the group average standard and target waveforms was comparable to previously reported results for the group average standard (Kerr et al., 2008), even though five fewer parameters were fitted. Despite the differences in fitting method between the two studies (due to the additional constraints available from the present data), only one parameter, the intrathalamic gain G_{srs}, differed considerably in value between Kerr et al. (2008) and here (Table 3).

Three parameters (N, the normalization factor; G_{ese}, the excitatory thalamocortical grain; and G_{esre}, the inhibitory thalamocortical gain) showed large differences between standard and target fits. By far the most notable change was in G_{ese}, which was nearly 30 times larger in targets than standards. By comparison, G_{esre} was approximately 2.5 times larger in targets than standards, while N was nearly twice as large.

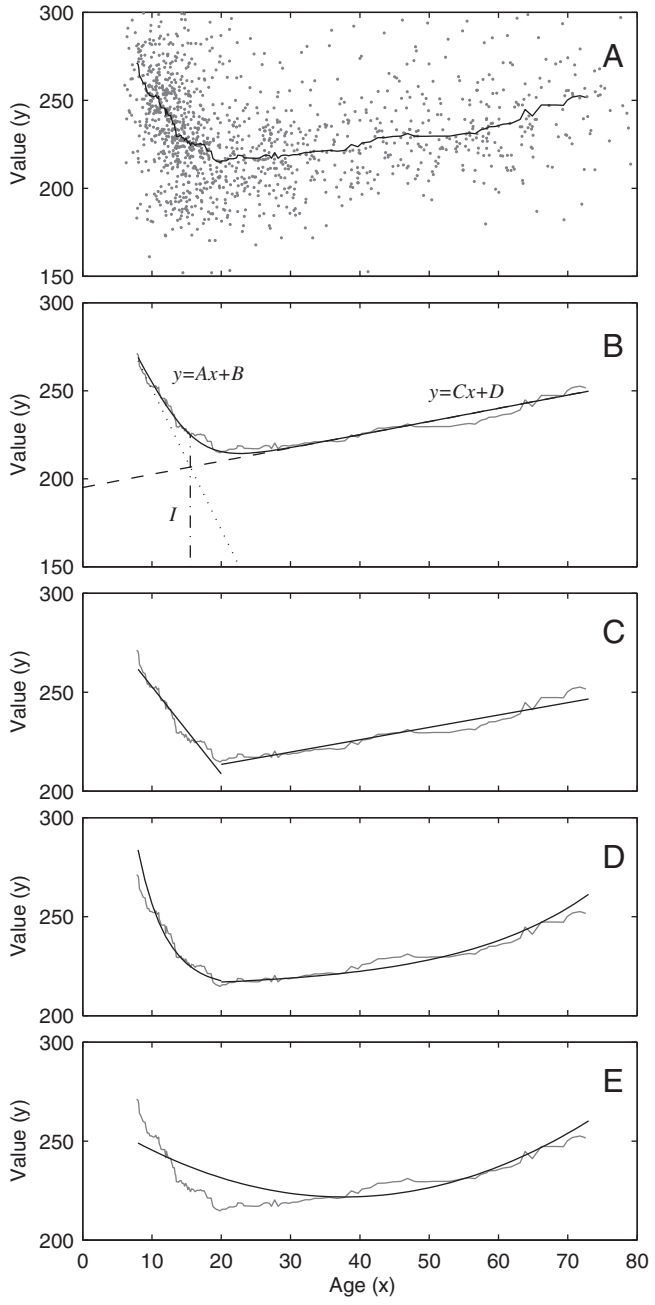

Fig. 3. Comparison of several possible fitting functions. (A) Example age trend data – target N2 component latency (in ms), from Kerr et al. (2010) – showing individual subjects (dots) and the moving median (solid line). (B) Schematic diagram of the line of best fit used here to determine age trends (solid black line). At young and old ages, it simplifies to the linear functions $y = Ax + B$ (dotted) and $y = Cx + D$ (dashed), respectively. The two straight lines intersect at age $x = I$ (dash-dotted), which is also the age of the maximum rate of change in slope of the fitting function. For comparison, the median of the experimental data (gray line) is also shown in this and subsequent panels. (C) Separate linear fits for development and aging trends, which produce a discontinuity at the crossover age of 20 years. (D) Separate exponential fits for development and aging trends, which overestimate the rates of change at both very young and very old ages. (E) Quadratic fit, which cannot accommodate the asymmetry between development and aging.

Differences between AEP and resting eyes-open EEG parameter values were also observed. Compared to resting EEG, both standard and target AEPs showed stronger intrathalamic gains (G_{srs}), a shift from excitation towards inhibition in all feedback parameters (X, Y, Z, and S), and smaller thalamocortical signal propagation times (t_0). The excitatory thalamocortical gain G_{ese} was weaker in standard AEPs than in resting EEG, while the inhibitory thalamocortical gain G_{esre} was stronger in target AEPs than in resting EEG.

3.2. Age trend fits

Age-related changes in waveforms were present throughout the entire age range, but were most rapid during development, with considerable changes in waveform morphology observed below age 20. Across all ages, fits to the moving average waveforms closely matched the major features of the data; several examples are shown in Fig. 4. Goodness-of-fit (as measured by χ^2) was best for age bins with a mean subject age of between 30 and 50 years; for standards, it was worst for bins with a mean age <10, while for targets it was worst for bins with a mean age between 15 and 30 years. No statistically significant sex differences were found; the results presented below are for the full dataset.

3.2.1. Stimulus and network properties

Age trends in the stimulus and network properties of the model are shown in Fig. 5 and Table 4. During development the normalization factor N decreased considerably in standards, and appeared to increase in targets, although this trend was not statistically significant. During aging, target N remained constant, while standard N increased approximately linearly, approaching the value for targets towards the upper limit of the age range used here.

The thalamocortical signal propagation time t_0 showed similar trends in both standards and targets, except the turning point for targets appeared to be somewhat earlier than that for standards ($I = 16$ and 25 years, respectively). In both standards and targets, t_0 decreased dramatically during development, and increased more slowly during aging. Target t_0 was slightly smaller than standard t_0 over the entire age range, but this difference was not statistically significant at any given age.

The spatial stimulus width r_s increased during development at similar rates in both standards and targets. During aging, target r_s continued to increase, while standard r_s showed no statistically significant change.

3.2.2. Gains

Age trends in the model gains are shown in Fig. 6 and Table 5. The cortical excitatory gain G_{ee} showed a considerable increase in strength during development in standards. The developmental changes in targets are difficult to interpret, and the significant scatter of points in this age range indicates that G_{ee} may in fact have a fairly constant small value ($\sim$1) during development. The cortical inhibitory gain G_{ei} presents a similar picture, with a large, significant increase in strength during development in standards, and large scatter during development in targets.

Both standards and targets show decreases in the strength of the excitatory thalamocortical gain G_{ese} during development, but this change is much larger in standards (95% decrease) than targets (25% decrease). Standards and targets also both show unusual trends in the strength of the thalamocortical inhibitory gain G_{esre}, including a rapid change from near-maximal values to near-minimal values in targets during middle age. This parameter requires cautious interpretation, as discussed in Section 4.3.2. The strength of the intrathalamic inhibitory gain G_{srs} was similar in standards and targets, both in terms of age trends and median values.

3.2.3. Feedback parameters

Age trends in the feedback parameters, shown in Fig. 7 and Table 6, result from the trends in gains. The age trends in the cortical feedback parameter X closely match the age trends in G_{ee}. During development, the thalamocortical feedback parameter Y changes from being positive to being near zero in both standards and

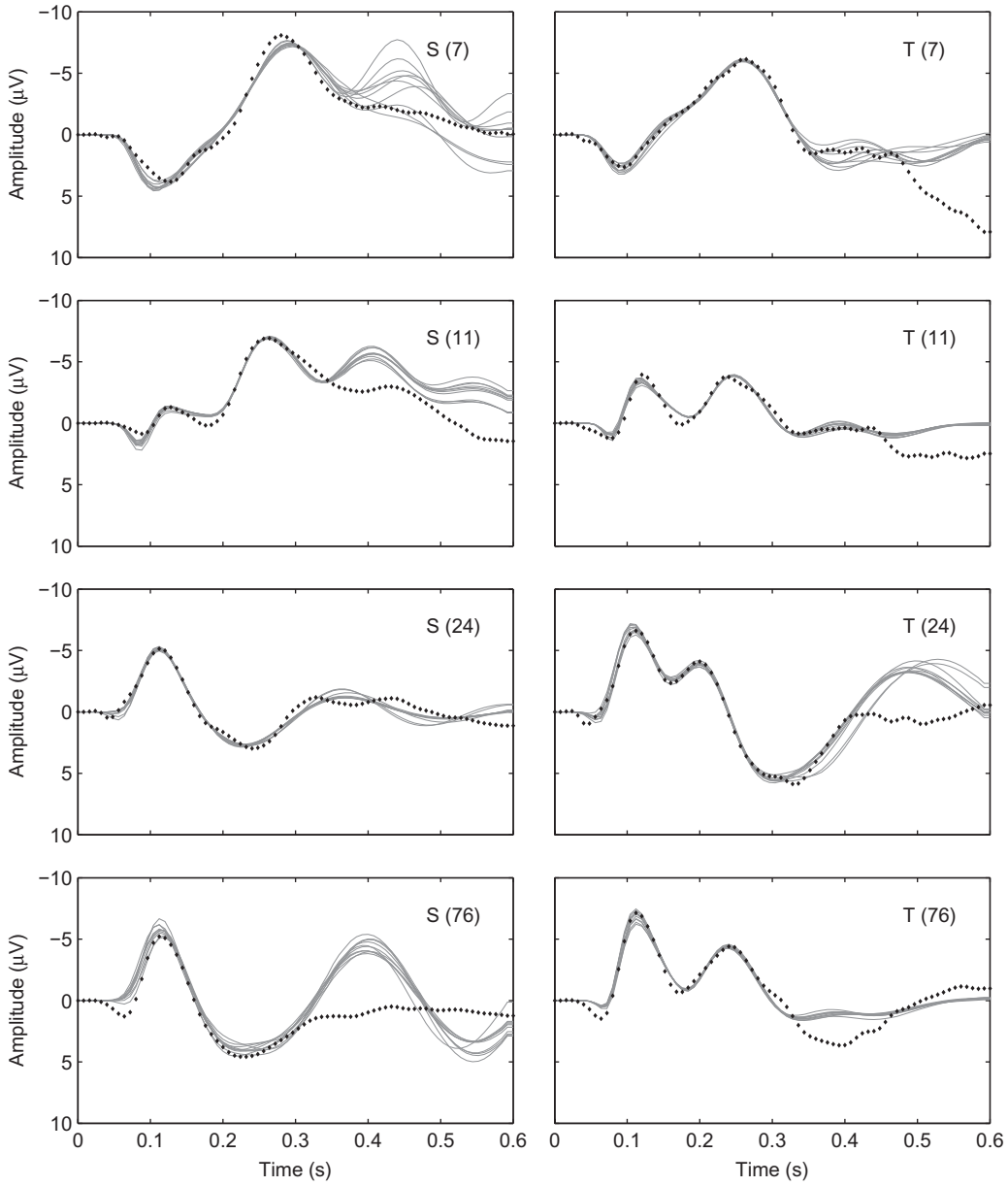

Fig. 4. Comparison of model fits (solid lines) to empirical waveform data (dots) for standards (left) and targets (right), at four characteristic ages: top row, 7 years; second row, 11 years; third row, 24 years; bottom row, 76 years. Relative to young adults (age 24), several striking age trends are evident: "inverted" standard and target responses (age 7), earlier maturation of targets compared to standards (age 11), and increased latency of target N2 and P3 (age 76). The model accurately reproduces all major features of the data up to approximately 350 ms, beyond which goodness-of-fit decreases in some cases, most likely due to a violation of the assumption that parameter values remain constant for the duration of the AEP.

targets. Although the magnitudes of these changes differ substantially, the median value in adults does not differ significantly between standards and targets. The intrathalamic feedback parameter Z is directly proportional to $-G_{srs}$, since in this study the values of α and β were not allowed to vary. The baseline stability parameter S increased during development in both standards and targets. However, during aging, standards and targets showed opposite trends, with S increasing in standards and decreasing in targets.

4. Discussion and summary

This study has used model-based fitting to provide information on the physiology underlying age trends in auditory oddball evoked potentials, using data collected from 1498 healthy subjects over an age range of 6–86 years. The approach applies the physiology-based neuronal activity model developed by Robinson and others (Robinson et al., 2002; Rennie et al., 2002; Kerr et al., 2008) to evoked potentials, providing a unified framework for analysis of both EEG and evoked potential phenomena (cf. van Albada et al., 2010). In contrast to phenomenological methods, such as component scoring, modeling allows specific and testable hypotheses to be formulated about the physiological changes that occur in the brain during development and aging. In addition to age trends, the differences in parameter values between standard and target AEPs were investigated; the effects of sex were also considered, but no statistically significant differences were found. This section discusses these results and uses them to make predictions about underlying physiology.

Crucially, modeling allows estimates to be made of quantities that are difficult or impossible to measure *in vivo* in humans. To

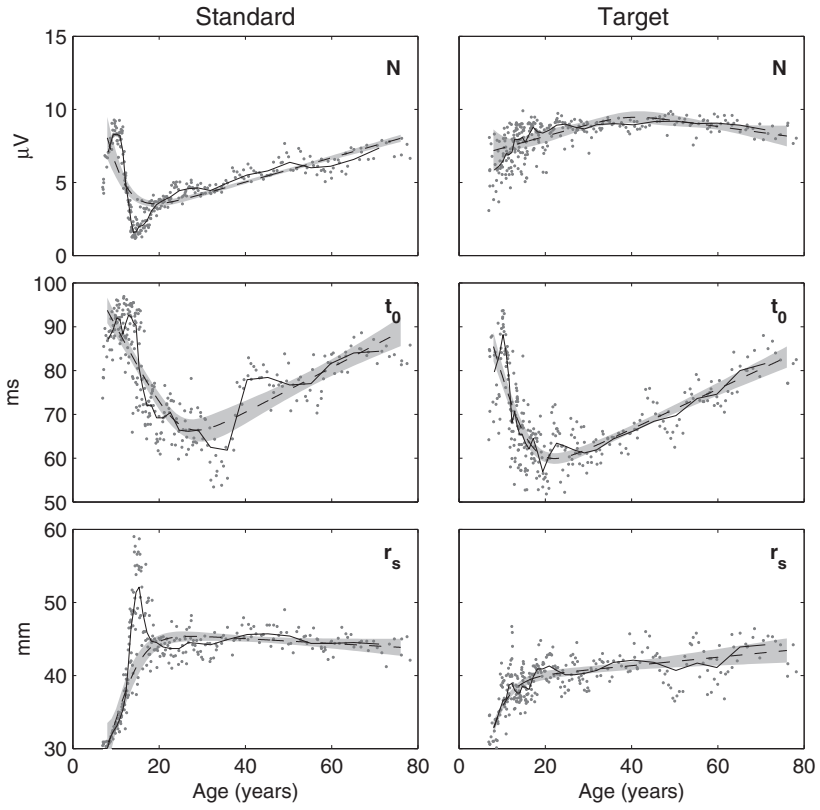

Fig. 5. Age trends in network parameters (labeled in each frame) for standards (left) and targets (right), showing values for each age bin (gray dots), lines of best fit (dashed lines) with 95% confidence intervals (shaded regions), and moving medians (solid lines). Line slopes and their significances are given in Table 4. The spike in standard r_s and corresponding dip in standard N during the ages of 13 to 17 is probably artifactual, as discussed in Section 4.3.1.

our knowledge, this study and its companion (van Albada et al., 2010) are the first to provide quantitative estimates of how neuronal connection strengths, thalamocortical signal propagation times, and stimulus properties change during development and aging. While it may eventually be possible to obtain more direct measurements of many (or even all) of the anatomical and physiological quantities described by the model parameters, modeling is currently the only approach that can provide estimates of these quantities.

Fits were good matches to data for at least the first 350 ms for both standards and targets across all ages, as shown in Fig. 4; thus, even the comparatively simple model used here was sufficient to explain all major features of the data, except target P3b. In comparison, other physiology-based models have focused on specific aspects of the auditory response, such as individual principal components (David et al., 2005; Kiebel et al., 2006) or the mismatch negativity (Garrido et al., 2007). The discrepancies between our model fits and some experimental waveforms after 350 ms suggest two future directions for development of the model. First, the present approximation of constant parameter values becomes less plausible as time from stimulus onset increases, due to effects such as thalamic gating and attentional focus; simple alternatives include linear, sigmoidal, or step-like changes between AEP and "resting-state" parameters. Second, AEP features of longer latency typically involve more complex interactions between brain regions, potentially including some that are not incorporated in the

Table 4
Age trends in network and stimulus model parameters: normalization factor N, thalamocortical signal propagation time t_0, and spatial stimulus width r_s. Values and standard errors are given for four measures: S_6, the slope of the fitted trend at age 6; S_{86}, the slope at age 86; M, the median value during early adulthood (ages 20–40); and I, the age at which the slope of the trend changes most rapidly.

Model	Fit	Standard	Target	Unit
N	S_6	-1.3 ± 0.8	0.1 ± 0.5	μV/year
	S_{86}	0.083 ± 0.007	-0.04 ± 0.04	μV/year
	M	4.4 ± 0.6	8.8 ± 0.6	μV
	I	10 ± 7	—	years
t_0	S_6	-1.8 ± 0.4	-3.5 ± 0.9	ms/year
	S_{86}	0.5 ± 0.1	0.46 ± 0.06	ms/year
	M	66 ± 6	62 ± 4	ms
	I	25 ± 6	16 ± 5	years
r_s	S_6	2.3 ± 0.6	2.2 ± 1.0	mm/year
	S_{86}	-0.03 ± 0.03	0.06 ± 0.03	mm/year
	M	44 ± 2	41 ± 2	mm
	I	—	8 ± 4	years

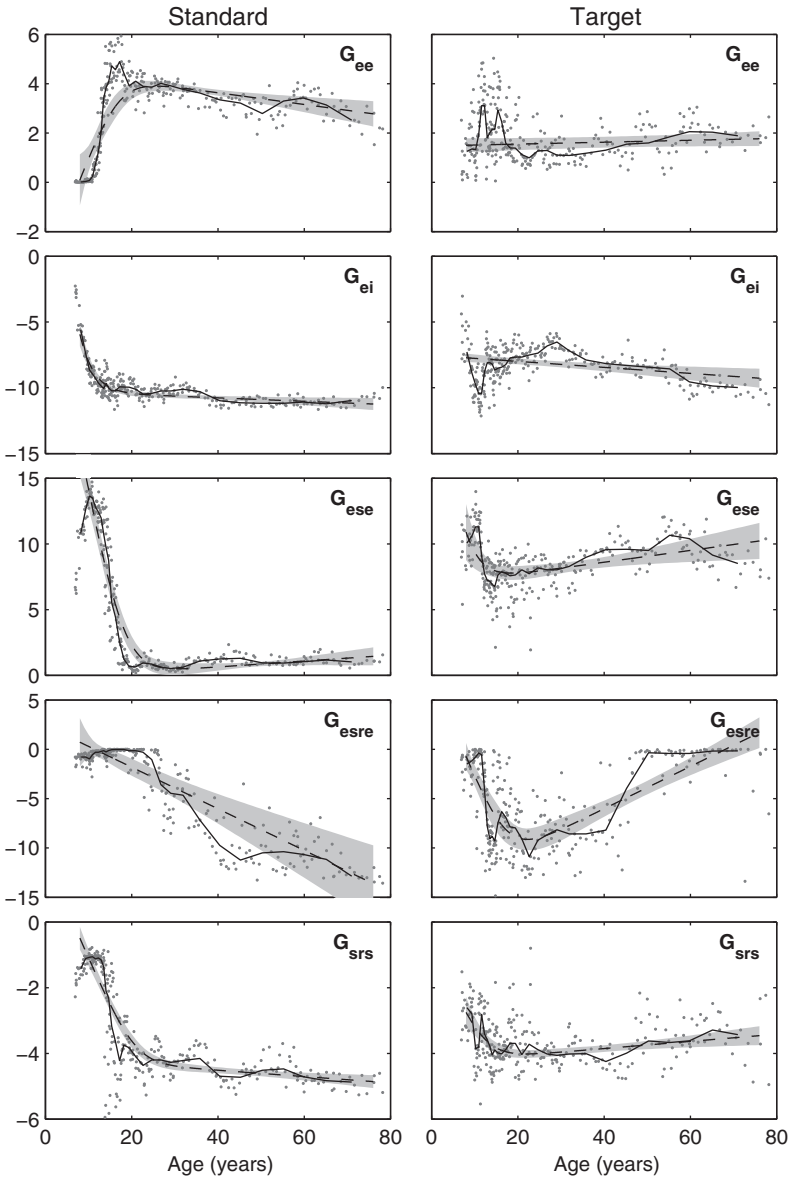

Fig. 6. Age trends in dimensionless gains (labeled in each frame) for standards (left) and targets (right), showing values for each age bin (gray dots), lines of best fit (dashed lines) with 95% confidence intervals (shaded regions), and moving medians (solid lines). Line slopes and their significances are given in Table 5.

version of the model used here, such as the hippocampus (Halgren et al., 1998).

We have shown that changes in AEP waveforms due to age and task conditions can be successfully explained by changes in model parameters, but the causes of these changes require further explanation. Two mechanisms exist that would be expected to produce parameter changes on the short time scales necessary for differentiation between standard and target stimuli (Kerr et al., 2008). First, changes in firing rates in the neuromodulatory system, including cholinergic, noradrenergic, and dopaminergic neurons, occur during attentional modulation (Schultz et al., 1997; Williams, 2005; Herrero et al., 2008). These changes would affect many model parameters, especially the gains (Clearwater et al., 2008), which were the only parameters found to differ significantly between standard and target AEPs. A second possibility is that standard and target AEPs are produced by distinct (or partially distinct) cortical networks; if their intrinsic parameter values differ, activation of these different networks would have effects similar to a parameter change in a single network. In addition to uncertainty regarding the extent to which each of these mechanisms contribute to the observed parameter changes, it is unknown what causative factors underlie them (i.e., what leads to the release of neurotransmitters and/or the activation of particular networks). Solving this problem would require detailed knowledge of information-processing aspects of the brain, including a computational model of novelty detection (Ranganath and Rainer, 2003), that is beyond the scope of the present work. In the interim, the present results can be interpreted with either of these mechanisms in mind.

4.1. Comparison with previous work

Parameter values for adult standard fits were generally similar to those obtained in Kerr et al. (2008), although several parameters showed statistically significant differences, due to the differences in methods used in the two studies. Only one waveform, the group average standard, was analyzed in the previous study, and this was not sufficient to fix any of the 13 model parameters to a single

Table 5
Age trends in the gain model parameters: excitatory cortical (G_{ee}), inhibitory cortical (G_{ei}), excitatory thalamocortical (G_{ese}), inhibitory thalamocortical (G_{esre}), and inhibitory intrathalamic (G_{srs}). Values and standard errors are given for four measures: S_6, the slope of the fitted trend at age 6; S_{86}, the slope at age 86; M, the median value during early adulthood (ages 20–40); and I, the age at which the slope of the trend changes most rapidly.

Model	Fit	Standard	Target	Unit
G_{ee}	S_6	0.7 ± 0.4	0.004 ± 0.004	per year
	S_{86}	-0.02 ± 0.01	0.004 ± 0.006	per year
	M	3.8 ± 0.4	1.1 ± 0.6	–
	I	–	–	years
G_{ei}	S_6	-2.2 ± 1.3	-0.02 ± 0.03	per year
	S_{86}	-0.01 ± 0.01	-0.02 ± 0.01	per year
	M	-10.3 ± 0.5	-7.4 ± 0.8	–
	I	4 ± 2	–	years
G_{ese}	S_6	-1.7 ± 0.6	-1.4 ± 1.0	per year
	S_{86}	0.02 ± 0.03	0.04 ± 0.03	per year
	M	0.8 ± 0.4	8.1 ± 1.3	–
	I	18 ± 7	–	years
G_{esre}	S_6	0 ± 13	-1.0 ± 1.0	per year
	S_{86}	-0.21 ± 0.08	0.21 ± 0.05	per year
	M	-3.0 ± 3.0	-8.7 ± 2.5	–
	I	–	17 ± 15	years
G_{srs}	S_6	-0.30 ± 0.07	-0.3 ± 0.2	per year
	S_{86}	-0.010 ± 0.006	0.011 ± 0.008	per year
	M	-4.2 ± 0.4	-4.0 ± 0.6	–
	I	21 ± 6	12 ± 10	years

value with confidence. Additionally, the only criteria that were available in that study to choose parameter values were goodness-of-fit and consistency with physiological estimates and EEG parameters. In contrast, the nearly 300 standard and target waveforms used in this study provided strict constraints on both the fit parameters and the fitting method itself. It was found that only eight fitted parameters were needed to model standard and target waveforms across the entire age range. The remaining five parameters were fixed, some to values outside the ranges found in Kerr et al. (2008), although all parameters were still well within physiological limits. This was necessary so that standards and targets, as well as age trends, could be fitted with the fewest possible param-

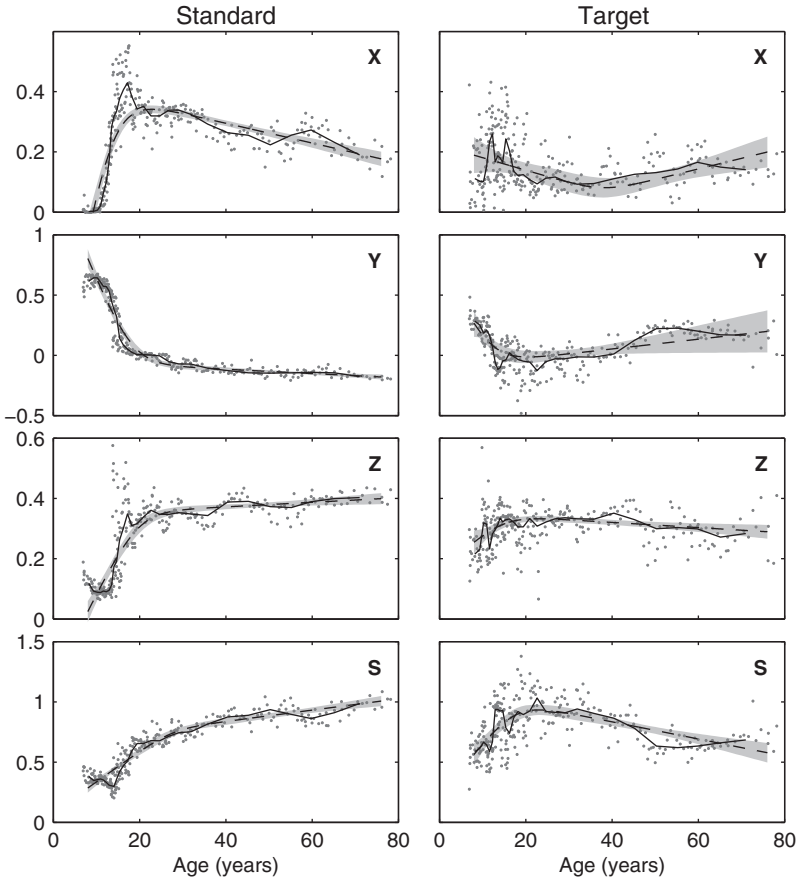

Fig. 7. Age trends in dimensionless feedback parameters (labeled in each frame) for standards (left) and targets (right), showing values for each age bin (gray dots), lines of best fit (dashed lines) with 95% confidence intervals (shaded regions), and moving medians (solid lines). Line slopes and their significances are given in Table 6.

Table 6
Age trends in feedback model parameters: cortical feedback *X*, thalamocortical feedback *Y*, intrathalamic feedback *Z*, and baseline stability *S*. Values and standard errors are given for four measures: S_6, the slope of the fitted trend at age 6; S_{86}, the slope at age 86; *M*, the median value during early adulthood (ages 20–40); and *I*, the age at which the slope of the trend changes most rapidly.

Model	Fit	Standard	Target	Unit
X	S_6	0.07 ± 0.03	-0.004 ± 0.006	per year
	S_{86}	-0.0033 ± 0.0007	0.004 ± 0.002	per year
	M	0.32 ± 0.04	0.10 ± 0.05	–
	I	13 ± 7	38 ± 38	years
Y	S_6	-0.08 ± 0.02	-0.1 ± 0.3	per year
	S_{86}	-0.0018 ± 0.0008	0.004 ± 0.004	per year
	M	-0.05 ± 0.05	0.0 ± 0.1	–
	I	18 ± 5	–	years
Z	S_6	0.028 ± 0.009	0.01 ± 0.02	per year
	S_{86}	0.0008 ± 0.0006	-0.0009 ± 0.0006	per year
	M	0.35 ± 0.03	0.33 ± 0.05	–
	I	20 ± 7	–	years
S	S_6	0.026 ± 0.005	0.04 ± 0.02	per year
	S_{86}	0.005 ± 0.002	-0.007 ± 0.003	per year
	M	0.73 ± 0.08	0.9 ± 0.2	–
	I	27 ± 9	17 ± 10	years

eters. All other tested combinations of fixed and fitted parameters either failed to produce smoothly varying age trends (suggesting over-parameterization), or failed to produce good fits to data over the full age range (suggesting under-parameterization), indicating that the set of initial parameter values and limits listed in Table 2 is optimal for the present purpose.

As shown in Table 3, only one fitted parameter (G_{srs}, the strength of the intrathalamic inhibitory gain) differed between resting EEG and both standard and target AEP fits, while a second parameter (G_{ese}, the strength of the thalamocortical excitatory gain) differed between resting EEG and standard AEP fits. The inhibitory thalamocortical gain G_{esre} differed between EEG fits and fits to the adult group average target, but this difference was not found for the median value *M* in early adulthood age trend fits (shown in Table 5), indicating that it may not be robust. These results indicate that both EEG and AEP phenomena can be obtained from strikingly similar locations in parameter space: changes between resting EEG and either target or standard AEP states correspond to changes in only a small number of parameters, a finding which is strong evidence of the model's fundamental validity.

In addition to the differences in fitted parameters described above, the values of two fixed parameters were significantly different from values obtained previously for resting EEG. The cortical damping rate γ was fixed to a much larger value ($400\ s^{-1}$) than found for resting EEG spectra ($70 \pm 30\ s^{-1}$) (Kerr et al., 2008). This parameter is the axonal transmission velocity divided by the characteristic axonal range. Since the axonal transmission velocity is unlikely to change substantially between the cortical networks responsible for EEG and AEP generation, we predict that the networks underlying AEPs have shorter axonal connections than those underlying ongoing EEG activity. Additionally, the dendritic rate constant α was fixed to a significantly smaller value ($12\ s^{-1}$) than found in EEG fits ($100 \pm 40\ s^{-1}$) (Kerr et al., 2008). We would thus predict that AEP networks depend more heavily on neurotransmitter receptors with slow kinetics, such as $GABA_B$ and NMDA glutamate receptors, as compared to the networks involved in producing resting EEG activity.

4.2. Task effects on parameters

To investigate the effects of task condition (i.e., standard or target stimuli) on parameter values, standard and target parameters were compared using two different methods: fits to the group average waveform of subjects aged 20–40, and the median values of fits to moving average waveforms over the same age range. This age range was chosen as it excludes the majority of both development and aging trends, so is least likely to be affected by these confounds. Only two parameters were found to have significantly different values in standards (S) and targets (T) using both methods: the excitatory thalamocortical gain G_{ese}, and the normalization factor *N*.

The main morphological difference between standard and target waveforms is the presence of an N2 component in targets, which is accounted for in the model by a significantly larger magnitude of $G_{ese}^{(T)}$ compared to $G_{ese}^{(S)}$, as shown in Tables 3 and 5. Physiologically, this result implies that N2 is the result of cortical activation caused by an excitatory thalamocortical feedback loop. This loop also appears to be strongly active in resting EEG, in which G_{ese} is also large (Rowe et al., 2004). In contrast, the value of G_{ese} is not statistically different from zero in standards, implying a suppression of the activity in this loop. A plausible functional interpretation of this framework is that target stimuli require further processing (and hence require excitatory feedback), whereas standard stimuli do not (and hence the brain needs to return to resting state in order to prepare for subsequent stimuli).

The larger magnitude of $N^{(T)}$ compared to $N^{(S)}$ implies a stronger gain from the brainstem to the cortex (via the thalamus) in targets as compared to standards. This is because neither of the other contributors to *N* – the stimulus amplitude at the level of the auditory nerve, or the conversion factor between neuronal firing rates and scalp potential – would be expected to change with task condition. This predicted change in gain may underlie aspects of the brainstem and/or thalamic components of the orienting response (Isa and Sasaki, 2002).

4.3. Age effects on parameters

All parameters showed at least one age trend in either standards or targets that was statistically significantly different from zero. In general, standard parameters changed more during development than during aging, while the opposite was true of target parameters. This suggests that, compared to standards, the targets are closer to adult form by age six, and are more heavily dependent on those cortical networks most vulnerable to the degenerative effects of aging. This view is consistent with findings that target component latencies increase more rapidly with age than standard component latencies (Kerr et al., 2010), and with an aging study by

Williams et al. (2008), which involved a wide range of psychometric and psychophysiological measures. This study concluded that early automatic responses (e.g., N1) were spared or even improved during aging, while later controlled responses (e.g., P3) declined with age.

4.3.1. Stimulus and network parameters

The normalization factor N in standards showed a large decrease during development, followed by a gradual increase during aging. In contrast, $N^{(T)}$ appeared to be nearly constant across age. While $N^{(S)}$ and $N^{(T)}$ differed by a factor of two during early adulthood, their values were similar at very young and very old ages. This finding may also be related to changes in the orienting response, which improves during development (Mezzacappa, 2004), but declines with age (Cabeza et al., 2004).

The changes in the thalamocortical signal propagation time t_0 in standards and targets are consistent with the changing amount and quality of myelin in the brain (Allison et al., 1983, 1984; Peters, 2002; Sowell et al., 2004). Specifically, myelination increases considerably during development, leading to increased transmission speeds (Sowell et al., 2004). Although axon lengths in the central nervous system increase during development, this effect is slight in children over the age of five (Ponton et al., 1993), and hence changes in myelination are likely to dominate the effect on t_0. There is conflicting evidence whether the amount of myelination declines during aging, whether its quality deteriorates, or both (Peters, 2002; Piguet et al., 2009), but in any of these cases, t_0 would be expected to increase during aging. These changes in t_0 provide a unified explanation of the decreases in latencies of the N2 and P3 components in targets during development, as well as their increases during aging.

The most dramatic age-related change in AEPs is the "inversion" of the waveform between young children and adults, in which the childhood waveform morphology (a positive component followed by a negative one) changes to adult morphology (a negative component followed by a positive one), as shown in Fig. 4. In the model, this change is largely produced by the increase in the spatial stimulus width r_s observed in both standards and targets. This parameter affects the dispersion of waves of neuronal activity in the modeled cortex; depending on the superposition of these waves, either an initial negativity or an initial positivity is produced.

The age range over which waveform inversion occurs (6–10 years) is similar to the age range during which neurofilaments in the superficial cortical layers mature (5–12 years) (Eggermont and Ponton, 2003), and these are similar to the ages during which r_s changes most rapidly, especially in targets. Neurofilament development would produce greater effective connectivity in the cortex, which would correspond to a larger value of r_s. Both $r_s^{(S)}$ and $r_s^{(T)}$ have similar values at age 6 (30–35 mm), and increase at similar rates until about age 12. The large "spike" seen in $r_s^{(S)}$ between the ages of 13 and 17 appears to be artifactual. Above a certain value (which depends on γ and r_{os}, but is approximately 45 mm in present case where $\gamma = 400\ \mathrm{s}^{-1}$ and $r_{os} = 150$ mm), further increases in r_s have little effect on the waveform other than decreasing its amplitude. Since N also modulates the waveform's amplitude, changes in these two parameters can counteract each other, leading to increased uncertainty in both. This effect is evident in Fig. 5, where the rapid increase in $r_s^{(S)}$ coincides with a rapid decrease in $N^{(S)}$.

4.3.2. Gains

The strength of both excitatory and inhibitory cortical gains (G_{ee} and G_{ei}, respectively) increased in standards during development. This suggests increased cortical involvement (but not necessarily activity) in the processing of standard stimuli during development. In contrast, $G_{ee}^{(T)}$ and $G_{ei}^{(T)}$ showed no clear age trends.

In standards, the excitatory thalamocortical gains G_{ese} decreased over the course of development from a near-maximal value to a value close to zero. In contrast, the developmental decrease in $G_{ese}^{(T)}$ was smaller, and appears to be complete by age 10. This suggests that G_{ese} is the parameter most responsible for the increasing difference between standard and target waveforms with age. Functionally, this result suggests the following interpretation: in young children, all stimuli result in positive feedback in the thalamocortical loop; however, this network is gradually "turned off" for standard stimuli, so only the behaviorally-relevant target stimuli lead to this additional activity.

The age trends in the inhibitory thalamocortical gain G_{esre} are striking for their large magnitudes and time courses, such as the step-like change in $G_{esre}^{(T)}$ during ages 40–50. These results should be interpreted with caution: the large scatter of data points in Fig. 6 suggests that G_{esre} is poorly constrained in this region of parameter space, and these age trends may not be robust.

The inhibitory intrathalamic gain G_{srs} showed only one significant age trend: a comparatively rapid increase in magnitude during development in standards. The role of G_{srs} is more difficult to discern than those of the other gains; large values of G_{srs} lead to spindle (15 Hz) activity (Robinson et al., 2005), but otherwise its effect is subtle. The thalamic reticular nucleus (TRN) has been implicated in the direction of attention (Mitrofanis and Guillery, 1993; Guillery et al., 1998), so it may appear surprising that there is not a greater difference between $G_{srs}^{(S)}$ and $G_{srs}^{(T)}$. However, if the TRN *causes* changes in attention, then it follows that G_{srs} would not initially differ between standards and targets, since until reaching the TRN these two stimuli would be treated similarly.

4.3.3. Feedback parameters

The gains discussed above can be combined into four feedback parameters (X, Y, Z, and S) that characterize the balance of excitation and inhibition in different areas of the brain, as described in Table 1 (Robinson et al., 2002). The cortical feedback parameter X shows similar age trends as G_{ee}, since G_{ei} does not change in targets and only changes in standards when $G_{ee} \approx 0$. The balance between excitation and inhibition in the thalamocortical loop, parameterized by Y, decreases considerably in standards during development, such that whereas this network provides net excitation below age 20, it provides net inhibition above that age. The age trends in $Y^{(T)}$ are not statistically significant. As stated in Section 3.2.3, age trends in the intrathalamic feedback parameter Z are equivalent to those in G_{srs}, since α and β are fixed.

Both X and Y parameters contribute to S, the stability of zero-frequency activity in brain. This parameter increases in both standards and targets during development. In general, the stability of a system parameterizes a tradeoff between quick reaction time (optimized by low stability) and quick recovery time (optimized by high stability). Increasing S during development suggests a change towards improved recovery time, and this change has been observed experimentally in terms of the interstimulus interval needed to elicit the N1 component (Čeponiené et al., 2002.)

4.4. Conclusions and future directions

To our knowledge, this paper provides the most comprehensive account of AEP generation using physiology-based models to date, as it accounts for all components except target P3b. Additionally, the physiological explanations given above suggest plausible mechanisms by which age-related changes in AEPs could arise. Many of these mechanisms – such as increased myelination during development leading to decreased latency – have previously been suggested as explanations of age trends in AEP component scores.

However, these explanations have tended to be quantitatively imprecise, and have often been based on unknown causative links. While the explanations given above are still tentative, they are more explicit than those typically offered to explain changes in component scores, and hence are more directly linked to the fundamental actions of drugs and intrinsic neuromodulators. For example, we make the predictions that (i) standard and target stimuli produce subcortical responses of similar magnitude in young children, but these magnitudes diverge during adolescence; (ii) neurons linking the thalamic sensory nuclei and the cortex are approximately an order of magnitude more excitable in response to target compared to standard stimuli; and (iii) myelination increases conduction velocity in thalamocortical fiber tracts by roughly 50% between the ages of 6 and 20. These predictions are more readily testable experimentally than are qualitative statements such as "increased myelination leads to decreased component latency". In future work, the findings presented here will be extended to additional electrodes, and will be compared to age trends obtained from evoked potential deconvolution (Kerr et al., 2010), EEG spectral fitting (van Albada et al., 2010), and alpha peak quantification (Chiang et al., 2008).

Acknowledgements

We acknowledge the data and support provided by BRAINnet (www.brainnet.net), which coordinates access to the Brain Resource International Database (www.brainresource.com) for independent scientific purposes. We also thank the individuals who gave their time to participate in the database. The Australian Research Council supported this work.

References

Albrecht R, von Suchodoletz W, Uwer R. The development of auditory evoked dipole source activity from childhood to adulthood. Clin Neurophysiol 2000;111:2268–76.
Allison T, Hume AL, Wood CC, Goff WR. Developmental and aging changes in somatosensory, auditory and visual evoked potentials. Electroencephalogr Clin Neurophysiol 1984;58:14–24.
Allison T, Wood CC, Goff WR. Brain stem auditory, pattern-reversal visual, and short-latency somatosensory evoked potentials: latencies in relation to age, sex, and brain and body size. Electroencephalogr Clin Neurophysiol 1983;55:619–36.
Bahramali H, Gordon E, Lagopoulos J, Lim CL, Li W, Leslie J, et al. The effects of age on late components of the ERP and reaction time. Exp Aging Res 1999;25:69–80.
Barajas JJ. The effects of age on human P3 latency. Acta Otolaryngol Suppl 1990;476:157–60.
Bartzokis G, Beckson M, Lu PH, Nuechterlein KH, Edwards N, Mintz J. Age-related changes in frontal and temporal lobe volumes in men: a magnetic resonance imaging study. Arch Gen Psychiatry 2001;58:461–5.
Benes FM, Turtle M, Khan Y, Farol P. Myelination of a key relay zone in the hippocampal formation occurs in the human brain during childhood, adolescence, and adulthood. Arch Gen Psychiatry 1994;51:477–84.
Brown WS, Marsh JT, LaRue A. Exponential electrophysiological aging: P3 latency. Electroencephalogr Clin Neurophysiol 1983;55:277–85.
Cabeza R, Daselaar SM, Dolcos F, Prince SE, Budde M, Nyberg L. Task-independent and task-specific age effects on brain activity during working memory, visual attention and episodic retrieval. Cereb Cortex 2004;14:364–75.
Čeponienė R, Rinne T, Näätänen R. Maturation of cortical sound processing as indexed by event-related potentials. Clin Neurophysiol 2002;113:870–82.
Chiang AKI, Rennie CJ, Robinson PA, Roberts JA, Rigozzi MK, Whitehouse RW, et al. Automated characterization of multiple alpha peaks in multi-site electroencephalograms. J Neurosci Methods 2008;168:396–411.
Clearwater JM, Kerr CC, Rennie CJ, Robinson PA. Neural mechanisms of ERP change: combining insights from electrophysiology and mathematical modeling. J Integr Neurosci 2008;7:529–50.
David O, Harrison L, Friston KJ. Modelling event-related responses in the brain. NeuroImage 2005;25:756–70.
de Graaf-Peters VB, Hadders-Algra M. Ontogeny of the human central nervous system: what is happening when? Early Hum Dev 2006;82:257–66.
Eggermont JJ, Ponton CW. Auditory-evoked potential studies of cortical maturation in normal hearing and implanted children: correlations with changes in structure and speech perception. Acta Otolaryngol 2003;123:249–52.
Freeman W. Mass action in the nervous system. New York: Academic Press; 1975.
Gallagher M, Colombo P. Ageing: the cholinergic hypothesis of cognitive decline. Curr Opin Neurobiol 1995;5:161–8.
Garrido MI, Kilner JM, Kiebel SJ, Friston KJ. Evoked brain responses are generated by feedback loops. Proc Natl Acad Sci USA 2007;104:20961–6.
Giedd JN. The teen brain: insights from neuroimaging. J Adolesc Health 2008;42:335–43.
Giedd JN, Blumenthal J, Jeffries NO, Castellanos FX, Liu H, Zijdenbos A, et al. Brain development during childhood and adolescence: a longitudinal MRI study. Nat Neurosci 1999;2:861–3.
Goodin DS, Squires KC, Henderson BH, Starr A. Age-related variations in evoked potentials to auditory stimuli in normal human subjects. Electroencephalogr Clin Neurophysiol 1978;44:447–58.
Gordon E, Cooper N, Rennie C, Hermens D, Williams LM. Integrative neuroscience: the role of a standardized database. Clin EEG Neurosci 2005;36:64–75.
Gratton G, Coles MGH, Donchin E. A new method for offline removal of ocular artifact. Electroencephalogr Clin Neurophysiol 1983;55:468–84.
Guillery RW, Feig SL, Lozsádi DA. Paying attention to the thalamic reticular nucleus. Trends Neurosci 1998;21:28–32.
Halgren E, Marinkovic K, Chauvel P. Generators of the late cognitive potentials in auditory and visual oddball tasks. Electroencephalogr Clin Neurophysiol 1998;106:156–64.
Herrero JL, Roberts MJ, Delicato LS, Gieselmann MA, Dayan P, Thiele A. Acetylcholine contributes through muscarinic receptors to attentional modulation in V1. Nature 2008;454:1110–4.
Isa T, Sasaki S. Brainstem control of head movements during orienting; organization of the premotor circuits. Prog Neurobiol 2002;66:205–41.
Johnstone SJ, Barry RJ, Anderson JW, Coyle SF. Age-related changes in child and adolescent event-related potential component morphology, amplitude and latency to standard and target stimuli in an auditory oddball task. Int J Psychophysiol 1996;24:223–38.
Kerr CC, Rennie CJ, Robinson PA. Physiology-based modeling of cortical auditory evoked potentials. Biol Cybern 2008;98:171–84.
Kerr CC, Rennie CJ, Robinson PA. Deconvolution analysis of target evoked potentials. J Neurosci Methods 2009;179:101–10.
Kerr CC, van Albada SJ, Rennie CJ, Robinson PA. Age trends in auditory evoked potentials via component scoring and deconvolution. Clin Neurophysiol 2010;121:962–76.
Key AP, Dove GO, Maguire MJ. Linking brainwaves to the brain: an ERP primer. Dev Neuropsychol 2005;27:183–215.
Kiebel SJ, David O, Friston KJ. Dynamic causal modelling of evoked responses in EEG/MEG with lead field parameterization. NeuroImage 2006;30:1273–84.
Lenroot RK, Giedd JN. Brain development in children and adolescents: insights from anatomical magnetic resonance imaging. Neurosci Biobehav Rev 2006;30:718–29.
Makeig S, Westerfield M, Jung TP, Enghoff S, Townsend J, Courchesne E, et al. Dynamic brain sources of visual evoked responses. Science 2002;295:690–4.
Marner L, Nyengaard JR, Tang Y, Pakkenberg B. Marked loss of myelinated nerve fibers in the human brain with age. J Comp Neurol 2003;462:144–52.
Mezzacappa E. Alerting, orienting, and executive attention: developmental properties and sociodemographic correlates in an epidemiological sample of young, urban children. Child Dev 2004;75:1373–86.
Mitrofanis J, Guillery RW. New views of the thalamic reticular nucleus in the adult and developing brain. Trends Neurosci 1993;16:240–5.
Moore JK, Guan YL. Cytoarchitectural and axonal maturation in human auditory cortex. J Assoc Res Otolaryngol 2001;2:297–311.
Nelder JA, Mead R. A simplex method for function minimization. Comput J 1965;7:308–13.
Nunez PL. Wave-like properties of the alpha rhythm. IEEE Trans Biomed Eng 1974;21:473–82.
Nunez PL. Neocortical dynamics and human EEG rhythms. New York: Oxford University Press; 1995.
Oades RD, Dittmann-Balcar A, Zerbin D. Development and topography of auditory event-related potentials (ERPs): mismatch and processing negativity in individuals 8–22 years of age. Psychophysiology 1997;34:677–93.
Peters A. Structural changes that occur during normal aging of primate cerebral hemispheres. Neurosci Biobehav Revl 2002;26:733–41.
Phillips AJ, Robinson PA. A quantitative model of sleep–wake dynamics based on the physiology of the brainstem ascending arousal system. J Biol Rhythms 2007;22:167–79.
Piguet O, Double KL, Kril JJ, Harasty J, Macdonald V, McRitchie DA, et al. White matter loss in healthy ageing: a postmortem analysis. Neurobiol Aging 2009;30:1288–95.
Ponton CW, Eggermont JJ, Coupland SG, Winkelaar R. The relation between head size and auditory brain-stem response interpeak latency maturation. J Acoust Soc Am 1993;94:2149–58.
Ponton C, Eggermont JJ, Khosla D, Kwong B, Don M. Maturation of human central auditory system activity: separating auditory evoked potentials by dipole source modeling. Clin Neurophysiol 2002;113:407–20.
Press WH, Flannery BP, Teukolsky SA, Vetterling WT. Numerical recipes in C. Cambridge: Cambridge University Press; 1992.
Ranganath C, Rainer G. Neural mechanisms for detecting and remembering novel events. Nat Rev Neurosci 2003;4:193–202.
Rennie CJ, Robinson PA, Wright JJ. Unified neurophysical model of EEG spectra and evoked potentials. Biol Cybern 2002;86:457–71.
Roberts JA, Robinson PA. Modeling absence seizure dynamics: implications for basic mechanisms and measurement of thalamocortical and corticothalamic latencies. J Theor Biol 2008;253:189–201.

Robinson PA, Rennie CJ, Rowe DL. Dynamics of large-scale brain activity in normal arousal states and epileptic seizures. Phys Rev E 2002;65:041924.
Robinson PA, Rennie CJ, Rowe DL, Connor SC, Gordon E. Multiscale brain modeling. Philos Trans R Soc B 2005;360:1043–50.
Robinson PA, Rennie CJ, Rowe DL, O'Connor SC. Estimation of multiscale neurophysiologic parameters by electroencephalographic means. Hum Brain Mapp 2004;23:53–72.
Robinson PA, Rennie CJ, Wright JJ. Propagation and stability of waves of electrical activity in the cerebral cortex. Phys Rev E 1997;56:826–40.
Robinson PA, Rennie CJ, Wright JJ, Bahramali H, Gordon E, Rowe DL. Prediction of EEG spectra from neurophysiology. Phys Rev E 2001;63:021903.
Rowe DL, Robinson PA, Rennie CJ. Estimation of neurophysiological parameters from the waking EEG using a biophysical model of brain dynamics. J Theor Biol 2004;231:413–33.
Saunders MG. Artifacts: activity of noncerebral origin in the EEG. In: Klass DW, Daly DD, editors. Current practice of clinical electroencephalography. New York: Raven; 1984. p. 37–67.
Scarff CJ, Reynolds A, Goodyear BG, Ponton CW, Dort JC, Eggermont JJ. Simultaneous 3-T fMRI and high-density recording of human auditory evoked potentials. Neuroimage 2004;23:1129–42.
Scherg M, Von Cramon D. Evoked dipole source potentials of the human auditory cortex. Electroencephalogr Clin Neurophysiol 1986;65:344–60.
Schultz W, Dayan P, Montague PR. A neural substrate of prediction and reward. Science 1997;275:1593–9.
Sowell ER, Thompson PM, Toga AW. Mapping changes in the human cortex throughout the span of life. Neuroscientist 2004;10:372–92.
Steriade M, Gloor P, Llinás RR, Lopes da Silva FH, Mesulam MM. Basic mechanisms of cerebral rhythmic activities. Electroencephalogr Clin Neurophysiol 1990;76:481–508.
van Albada SJ, Gray RT, Drysdale PM, Robinson PA. Mean-field modeling of the basal ganglia-thalamocortical system. II. Dynamics of parkinsonian oscillations. J Theor Biol 2009;257:664–88.
van Albada SJ, Kerr CC, Chiang AK, Rennie CJ, Robinson PA. Neurophysiological changes with age probed by inverse modeling of EEG spectra. Clin Neurophysiol 2010;121:21–38.
van Albada SJ, Rennie CJ, Robinson PA. Variability of model-free and model-based quantitative measures of EEG. J Integr Neurosci 2007;6:279–307.
van Albada SJ, Robinson PA. Mean-field modeling of the basal ganglia-thalamocortical system. I. Firing rates in healthy and parkinsonian states. J Theor Biol 2009;257:642–63.
Volkow N, Logan J, Fowler J, Wang G-J, Gur R, Wong C, et al. Association between age-related decline in brain dopamine activity and impairment in frontal and cingulate metabolism. Am J Psychiatry 2000;157:75–80.
Williams LM. An integrative neuroscience model of ''significance'' processing. J Integr Neurosci 2005;5:1–47.
Williams LM, Gatt JM, Hatch A, Palmer DM, Nagy M, Rennie C, et al. The Integrate model of emotion, thinking, and self regulation: an application to the ''paradox of aging''. J Integr Neurosci 2008;7:367–404.
Wilson HR, Cowan JD. A mathematical theory of the functional dynamics of cortical and thalamic nervous tissue. Kybernetik 1973;13:55–80.
Wright JJ, Liley DTJ. Dynamics of the brain at global and microscopic scales: neural networks and the EEG. Behav Brain Sci 1996;19:285–94.